Supporting Information for

Water Dynamics in Nanoporous Silica: Ultrafast Vibrational Spectroscopy and Molecular Dynamics Simulations

Steven A. Yamada,[†] Jae Yoon Shin,[†] Ward H. Thompson,[‡]* and Michael D. Fayer[†]*

[†]Department of Chemistry
Stanford University, Stanford, CA 94305, USA
*Phone: 650 723-4446; Email: fayer@stanford.edu

[‡]Department of Chemistry
University of Kansas, Lawrence, KS 66045, USA
*Phone: 785 864-3980; Email: wthompson@ku.edu

I. Experimental Procedures

A. Particle Size Reduction.

In preliminary optical experiments, the as-received MCM41 powder generated considerable scattered light. The excitation pulses were centered at $\lambda \simeq 4.8$ μm. With particle diameters in the > 1 μm range (according to Sigma Aldrich), the condition for Mie scattering, comparable wavelength and particle size, was well satisfied.[1] Several approaches were used to decrease the intensity of the scattered light. First, the particle size was reduced. In the Mie regime, the intensity of the forward scattered electric field grows with particle diameter.[1] In 3rd order optical experiments, scatter signals are observed when the momenta of the pump fields are shifted into the direction of the probe beam (separated by a small crossing angle relative to the pump). This process is combatted by reducing the probability of forward scattering.

Sedimentation was employed to select smaller particle diameters from the intensely scattering (as-received) powders. The settling velocity, v, of a spherical particle under arbitrary flow conditions is

$$v^n = \frac{4}{3}\frac{g}{k(n)}\left[\frac{\rho_s - \rho}{\rho^{n-1}}\right]\mu^{n-2}d^{3-n}, \qquad \text{(S1)}$$

where g is the acceleration due to gravity, $k(n)$ is a constant term that is a function of the state of flow n, d is the diameter, μ is the dynamic viscosity, and ρ_s and ρ are the densities of the particle and the liquid, respectively.[2] The value n ranges from 1 for laminar flow (Stokes' law) to 2 for turbulent flow (Newton's law). Any intermediate value of n represents a transitional flow regime.[2] The resistance of a particle in a fluid is quantified by the coefficient of drag

$$C_d = k(n)\,\mathrm{Re}^{n-2}, \tag{S2}$$

where $\mathrm{Re} = dv\rho/\mu$ is Reynolds number. According to Eq. (S2), in the Stokes' limit C_d is inversely proportional to Reynolds number, while in Newton's limit it is constant. Taking the silica particles to be sufficiently small spheres, their settling velocity in a lower density fluid is governed by Stokes' law,[2]

$$v = \frac{gd^2}{18}\left[\frac{\rho_s - \rho}{\mu}\right], \tag{S3}$$

for which $n = 1$. Stokes' law is accurate when viscous forces dominate inertial forces, or when $\mathrm{Re} \ll 1$.[2] From nitrogen adsorption/desorption measurements, the total pore volume of MCM41 was found to be 0.91 ± 0.07 cm^3/g. The density of water occupying nm size silica pores has been estimated to be ~10% lower (~0.9 cm^3/g) than in the bulk state.[3] The density of amorphous silica is ~2.2 g/cm^3.[4] These values lead to an estimated average water-filled particle density of ρ_s = 1.33 g/cm^3. Thus, the applicability of Stokes' limit ($\mathrm{Re} \ll 1$) is found to be reasonable for particle diameters $\ll$ 177 μm for MCM41 settling in liquid water. Then, $v \propto d^2$ as in Eq. (S3).

The as-received MCM41 particles were placed on top of a long column of water and allowed to sediment for at least 10 min. Following 10 min, the top fraction, ~8 in or 20 cm of water, was vacuum filtered and the remaining particles were allowed to dry. The particles were then collected for later use. The length of the collected portion of the column and the settling time used gave a selection velocity, v_{select} = 3.3 x 10^{-4} m/s. Particles with $v > v_{select}$, or diameters greater than d_{select} = 43 μm were, in principle, not collected. The yield of smaller diameter particles was small. Repeating the procedure several times produced a sufficient number of particles to perform all experiments of interest. A significant reduction in scattered light was observed following reduction of the particle size in this manner, consistent with the predictions of Mie scattering theory.[1]

B. Surface Area, Pore Size Distribution, and Pore Volume of MCM41.

A standard method used to characterize mesoporous silica materials is measurement of the adsorption and desorption of an inert gas, typically N_2 (g), on the material at fixed temperature.[5,6] The nitrogen sorption isotherms shown in Fig. S1A were collected at 77 K on the as-received and smaller diameter MCM41 particles, obtained according to the procedure described in Section A. The experiments were performed on an Autosorb iQ_3 gas sorption instrument (Quantachrome) located at the Soft & Hybrid Materials Facility (SMF) at the Stanford Nano Shared Facilities (SNSF). No differences in the geometric characteristics of the internal pore structures were observed when the particle size was reduced. Therefore, the measured dynamics in the smaller MCM41 particles should be identical to those in the as-received particles.

Fig. S1B shows BET plots obtained from the adsorption curves in Fig. S1A. The slope and intercept of the linear plots are functions of v_m, the volume of gas needed to form a complete unimolecular adsorbed layer, and C, a constant related to the heat of adsorption of this layer.[5] The specific BET surface area is calculated from v_m according to

$$S_{BET} = \frac{v_m N_A \sigma}{mV}, \tag{S4}$$

where N_A is Avogadro's number, σ is the molecular cross-sectional area of N_2 (g) (16.2 Å^2),[7] m is the mass of the MCM41 sample, and V is the molar volume of N_2 (g) at STP. Using Eq. (S4), the specific BET surface area was calculated to be S_{BET} = 960 ± 30 m^2/g. This value is consistent with previous measurements on MCM41 samples with similar pore diameters.[8,9] Pore diameter distributions, shown in Fig. S1C, were obtained by performing BJH analysis[6] on the sorption isotherm curves in Fig. S1A. Analysis of the adsorption or desorption curves gave identical results. The pore diameter, D, was found to be 2.5 ± 0.2 nm, within the range specified by Sigma Aldrich, by fitting the distributions with a Gaussian function of diameter. The primary mesopore volume,[8,9] determined at P/P_0 = 0.55, was 0.8 ± 0.1 cm^3/g. The total pore volume was 0.91 ± 0.07 cm^3/g, determined at the highest P/P_0.

C. Sample Hydration.

Solutions and powders described in this section were prepared and manipulated under an N_2 (g) atmosphere. Dry potassium selenocyanate was dissolved in deuterium oxide at 0.3 M as previously described.[10] The solution was introduced into MCM41 powder (~10-30 mg) that was previously dried on a Schlenk line under vacuum (~100 mTorr) at ~200 ˚C for a few days. The powders were gently mixed in the 0.3 M KSeCN/D_2O solution for at least 20 min. The particles were then vacuum filtered for 2 min to remove bulk solution from the sample. The filtered particles were collected into a 20-mL scintillation vial that was sealed with an airtight rubber septum. The scintillation vial was connected to a home-built hydration chamber (Fig. S2). Nitrogen gas containing D_2O vapor, maintained at a fixed relative humidity, was flowed over the silica sample overnight to hydrate the pores. The water adsorption/desorption isotherms for MCM41 have been reported.[3,11] The D_2O vapor pressure in the hydration chamber was fixed above the threshold pressure for capillary condensation. The MCM41 samples were hydrated at either 100% or 78% RH by bubbling the N_2 stream through pure D_2O or D_2O saturated with NaCl, respectively, before the sample. At fixed temperature, saturated salt solutions provide a simple and robust way to maintain a fixed vapor pressure, and their properties have been extensively tabulated.[12] At P/P_0 just beyond capillary condensation, the uniform primary mesopores of diameters 2.5 ± 0.2 nm are completely filled with water. In the post capillary condensation region (P/P_0 > ~0.6), MCM41 displays a second region of hydration. The mass increase from 78% to 100 % RH is ~8%.

D. Sample Cell Preparation and Linear IR Spectroscopy.

Following hydration of the powder overnight, the sample was prepared in a N_2 (g) glovebox to avoid H_2O contamination and exposure of $SeCN^-$ to oxygen. The sample cell consisted of two 3 mm thick, 25.4 mm diameter CaF_2 windows with a 25 μm path length between them. The gap was maintained with two concentric 25 μm thick polytetrafluoroethylene (PTFE) spacers with outer diameters of 25.4 mm and 13 mm, respectively. The inner diameter of the smaller spacer was ~ 8 mm. The two spacers were placed on top of one window with all three centers aligned. The sample was evenly applied within the circular area enclosed by the smaller spacer. A layer of paraffin oil, used as an index matching fluid, was applied over the sample and entire window. The second window was lowered on top of the first, sandwiching the paraffin oil

coated sample between the windows. The hydrophobic paraffin oil coats the particles rather than displacing the aqueous solution in the pores, filling the gas filled voids between particles. The refractive index gradient between the hydrated silica particles (~1.4) and gas voids (1.00) is significant. Reducing this gradient with an index matching fluid reduced the scattered light observed in the optical experiments. The second purpose of the paraffin oil was to maintain the hydration state of the powder over a long period of time (weeks). Fourier Transform IR (FT IR) spectra of the KSeCN/D_2O containing MCM41 were measured with a Thermo Scientific Nicolet 6700 FT IR spectrometer purged with CO_2 and H_2O free air. The absorption spectrum of the silica powder containing solely D_2O with identical spacer thicknesses was measured. The non-resonant spectrum was subtracted from the resonant spectrum to yield the isolated CN stretch absorption in nanoconfined D_2O. In most cases, a small linear baseline was subtracted from the difference spectrum to account for a minor slope in the baseline.

E. Polarization-Selective Pump Probe Spectroscopy with Scatter Reduction.

In polarization selective pump-probe (PSPP) spectroscopy, the time delay separating the first two pulses in the general 2D IR pulse sequence, t_1, is fixed to zero (Fig. 1C). The first two sample-field interactions occur simultaneously with the arrival of a single pump pulse. The third interaction occurs when the probe pulse arrives an interval, t_2, later. The PP signal is the transient difference in the probe intensity with the pump pulse on versus off.[13] To acquire the signal, the pump is chopped at 500 Hz, or half the laser repetition rate, with an acousto-optic modulator (AOM; see below). In the simplest implementation, the acquired signal can be expressed as

$$S(t_2,\omega_3)=\frac{S_{on}(t_2,\omega_3)-S_{off}(\omega_3)}{S_{off}(\omega_3)}, \tag{S5}$$

where the subscripts *on* and *off* refer to the PP signals acquired with the pump present or absent, t_2 is the delay between pump and probe, and ω_3 is the detection frequency. However, Eq. (S5) is not ideal, as it is strongly susceptible to scatter from the pump pulse. The total detected intensity on a square law detector in the presence of scatter can be written

$$\begin{aligned} S_{on} &\propto \left|E_{pr}+E_s+sE_p\right|^2 \\ &= S_{off}+\left|sE_p\right|^2+E_{pr}E_s^*+s^*E_{pr}E_p^*+s^*E_sE_p^*+(c.c.), \end{aligned} \tag{S6}$$

where E_{pr}, E_s, and sE_p refer to probe, signal, and scattered pump fields (s is a complex scatter coefficient), respectively, $S_{off} = \left|E_{pr}\right|^2$, and the small homodyne signal, $\left|E_s\right|^2$, has been neglected. The explicit time-dependence of the terms has been omitted. The PP signal is the term $E_{pr}E_s^*$. The first term, S_{off}, is routinely subtracted (Eq. (S5)), leaving three scatter terms.

The following data acquisition scheme was used to eliminate the two phase-dependent (heterodyne) scatter terms $s^*E_{pr}E_p^*$ and $s^*E_sE_p^*$,

$$S(t_2,\omega_3) = \frac{S_{on}(\phi=0,t_2,\omega_3) + S_{on}(\phi=\pi,t_2,\omega_3) - 2S_{off}(\omega_3)}{2S_{off}(\omega_3)}, \tag{S7}$$

where the absolute phase, ϕ, of the pump was cycled between 0 and π with an AOM pulse shaper.[14,15] When ϕ is flipped by π, only the phase-dependent scatter terms (Eq. S6), which depend on the absolute phase of the pump pulse, change their sign and are eliminated in Eq. (S7). The homodyne scatter, $\left|sE_p\right|^2$, is independent of t_2 and is removed by baseline subtraction of the data at negative t_2.

In principle, Eq. (S7) should eliminate heterodyne scatter, but a strongly scattering sample combined with experimental noise necessitates extensive averaging. In the presence of noise, the scatter terms fluctuate shot to shot, resulting in residual scatter after application of Eq. (S7). Residual heterodyne scatter appears as a modulation in t_2, especially obvious when the signal is small compared to the scatter signals. In a typical PSPP experiment, the sampling rate of the population period, t_2, is below the Nyquist rate for un-aliased detection of the scatter optical frequency. At 2092 cm^{-1} (one half-width above line-center), the optical period is 15.9 fs, requiring one sample per ~8 fs.

For strongly scattering samples, a new method was implemented in which, for a desired delay t_2, a small range of values, $t_2 - \tau_1 \rightarrow t_2 + \tau_1$, was densely sampled. If the range $2\tau_1$ is equivalent to an integral number of optical cycles, and if it is small compared to the decay rate of the PP signal or scatter interferogram envelope, averaging of the data eliminates the scatter fringes and retains the PP signal at time t_2. To implement this routine, precise control of the time delay on the order of a few fs is required. Such control is beyond the specifications of the mechanical delay stage setting the probe pulse timing, but easily attainable with the AOM pulse

shaper controlling the pump timing.[14,16] A schematic of the mid-IR AOM configured in a 4-*f* pulse shaping geometry is shown in Fig. S3. For each laser shot, an acoustic wave, consisting of a 75 MHz carrier that is amplitude and phase modulated, is launched into a germanium window.[14,16,17] The window is filled by the waveform before the arrival of the pump. Before reaching the window, the input pump pulse is dispersed by a grating tilted down toward a spherical mirror (f = 20 cm) one focal length away. The spherical mirror collimates the dispersion and focuses the frequency components into the germanium window for enhanced frequency resolution. The fundamental operation of the AOM is to multiply the input spectrum, $E_{in}(\omega)$, by a mask function, $M(\omega)$, in the frequency domain, or

$$E_{out}(\omega) = M(\omega)E_{in}(\omega). \tag{S13}$$

The following mask function was applied to delay the single pump pulse in the PP experiment:

$$M(\omega) = e^{-i\omega\tau_1}e^{i\phi}, \tag{S14}$$

where the pump is delayed to $-\tau_1$ relative to its usual arrival time (exactly t_2 before the probe), and ϕ is the absolute phase applied to the pump which appears in Eq. (S7). The output pulse in time is reassembled on the output side of the AOM window, which is the mirror image of the input side. Whereas the input performs the Fourier transform $E_{in}(t) \rightarrow E_{in}(\omega)$, the output performs the inverse Fourier transform $M(\omega)E_{in}(\omega) \rightarrow E_{out}(t)$.

The PP data acquisition was modified in the following way for strongly scattering samples. At each delay, t_2, the pump pulse was scanned from $\tau_1 = -\epsilon \rightarrow \tau_1 = +\epsilon$, which corresponds to $t_2 - \epsilon \rightarrow t_2 + \epsilon$ (Fig. S3). In all experiments, ϵ = 100 fs was chosen, which is slightly greater than 6 optical cycles. This range was sampled in 2 fs increments, well-above the required Nyquist rate for the highest frequency of interest. The data without (blue curves) and with (red curves) phase cycling (Eq. (S7)) are displayed in Fig. S3B. The data over an integral number of optical cycles (6 or fewer) were averaged together to obtain the scatter-free PP signal at delay t_2 (Fig. S3B, black lines).

II. Data

A. Isotropic Pump-Probe Signals.

The isotropic pump-probe decays ($P(t_2) = [S_{\parallel}(t_2) + 2S_{\perp}(t_2)]/3$) for $SeCN^-$ in bulk D_2O (black points) and D_2O confined in MCM41 (red points: 100% RH; green points: 78% RH) are shown in Fig. S4 near the peak of the absorption spectrum (2075.6 cm^{-1}). The single exponential decays reflect the lifetime of the vibrationally excited CN stretching mode. The lifetime of the CN stretch in confined D_2O is identical within experimental error to the lifetime in bulk D_2O, previously reported to be 36.2 ps.[10]

B. Tables of Parameters.

Table S1. Orientational Relaxation Parameters.

Sample	A_1	t_1 (ps)	A_2	t_2 (ps)	A_3	t_3 (ps)	τ_c (ps)
Pore 78% RH	0.08 ± 0.05	2 ± 1	0.26 ± 0.05	6 ± 1	0.03 ± 0.01	50 ± 20	9 ± 1

Table S2. CLS Parameters.

Sample	A_1	τ_1 (ps)	A_2	τ_2 (ps)	A_3	τ_3 (ps)	τ_c (ps)
Pore 78% RH	0.26 ± 0.02	0.9 ± 0.2	0.29 ± 0.04	2.6 ± 0.4	0.08 ± 0.01	14 ± 1	3.2 ± 0.3

Table S3. FFCF Parameters.

Sample	T_2 (ps)	Γ (cm^{-1})	Δ_1 (cm^{-1})	τ_1 (ps)	Δ_2 (cm^{-1})	τ_2 (ps)	Δ_3 (cm^{-1})	τ_3 (ps)
Pore 78% RH	1.5 ± 0.3	8 ± 1	8.8 ± 0.2	0.8 ± 0.2	8.8 ± 0.8	2.6 ± 0.4	4.0 ± 0.3	14 ± 1

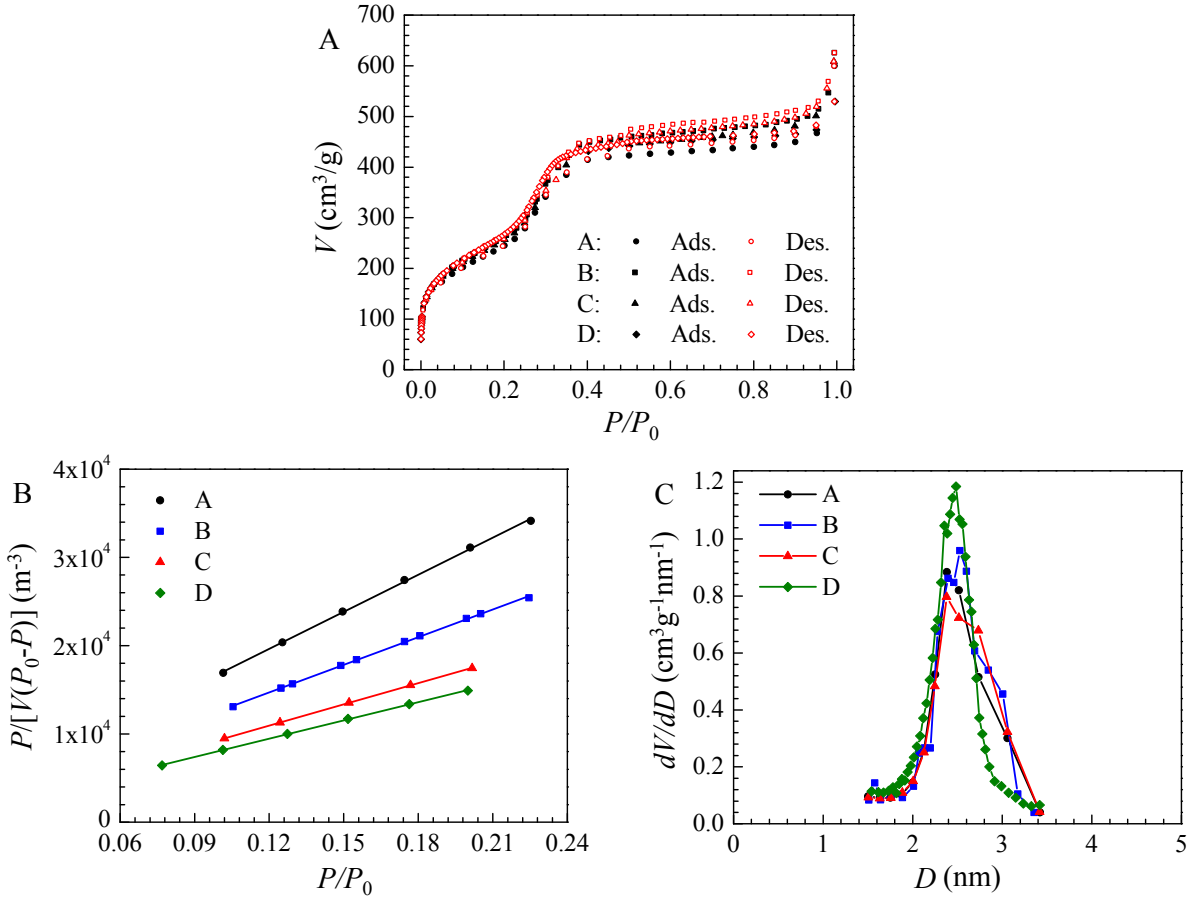

Figure S1. A. N_2 (g) adsorption (Ads.) and desorption (Des.) isotherms of four independently prepared MCM41 samples. Sample C is a small particle sample. The remaining samples were measured as-received. The sorption isotherms are consistent. **B.** BET plots obtained from the adsorption curves in A. The specific BET surface area is 960 ± 30 m^2/g. **C.** Pore diameter distributions obtained from BJH analysis of the curves in A. The pore diameter is 2.5 ± 0.2 nm. The primary mesopore volume is 0.8 ± 0.1 cm^3/g.

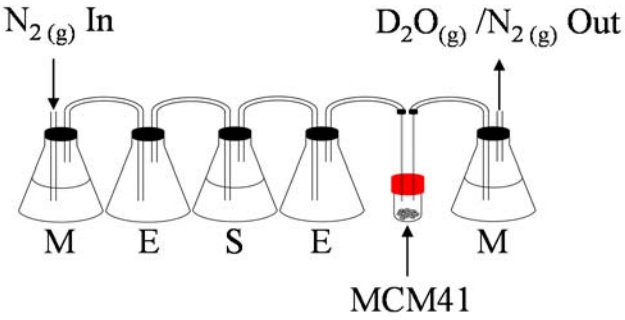

Figure S2. Homebuilt flow chamber used to control the hydration state of $SeCN^-/D_2O$ containing MCM41 silica: M = Mineral Oil, E = empty, S = D_2O or saturated NaCl/D_2O. For clarity, only one S containing flask is depicted, whereas two were typically used in series to ensure complete humidification of the N_2 stream.

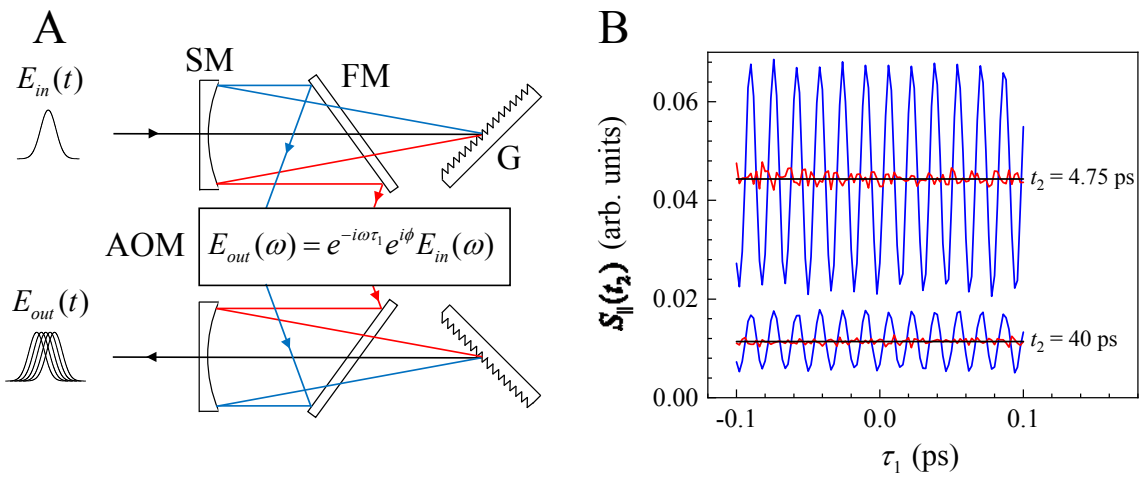

Figure S3. A Mid-IR pulse shaping system featuring a germanium acousto-optic modulator (AOM) in a 4-*f* geometry. G: grating, SM: spherical mirror, FM: folding mirror. In PSPP experiments, the input pump spectrum, $E_{in}(\omega)$, is multiplied by a mask function, $M(\omega) = e^{-i\omega\tau_1} e^{i\phi}$, which allows for phase cycling and the ability to delay the pulse in time. B The observed parallel pump-probe signal, $S_{\|}(t_2)$, obtained when the delay is scanned from $t_2 - \tau_1$ to $t_2 + \tau_1$ (τ_1 = 100 fs) at two times: t_2 = 4.75 ps and t_2 = 40 ps. blue: no phase cycling, red: phase cycling, black: PP signal level following averaging of data with phase cycling (red) over 6 optical cycles. Heterodyne scatter terms oscillate as t_2 is scanned (blue), while the signal is constant (black). Homodyne scatter has been subtracted from the data obtained at negative t_2 delays; the black horizontal lines reflect the baselined signal.

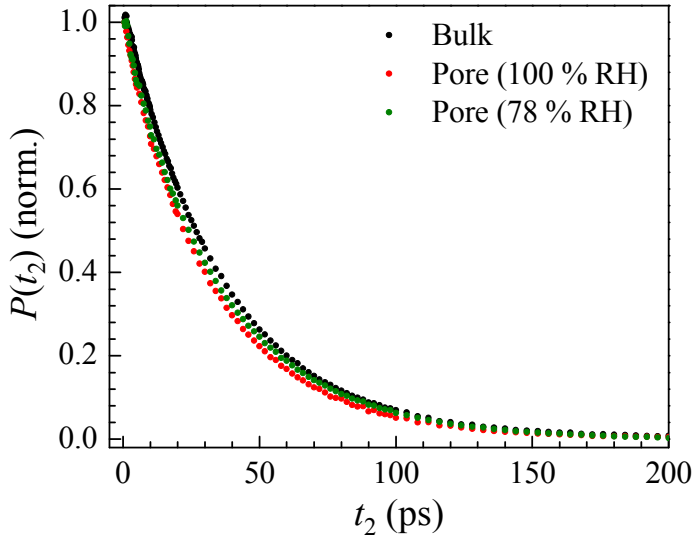

Figure S4. Isotropic PP Signals of $SeCN^-$ in bulk D_2O (black points) and in D_2O confined in the silica pore (red points: 100% RH; green points: 78% RH) near the peak of the absorption spectrum (2075.6 cm^{-1}). The curves are normalized to the value of the data at t_2 = 0.5 ps.

References

(1) Bohren, C. F.; Huffman, D. R. In *Absorption and Scattering of Light by Small Particles*; Bohren, C. F., Huffman, D. R., Eds. 2007.

(2) McGauhey, P. H. Theory of Sedimentation. *J. Am. Water Works Assoc.* **1956**, *48*, 437-448.

(3) Kocherbitov, V.; Alfredsson, V. Hydration of MCM-41 Studied by Sorption Calorimetry. *J. Phys. Chem. C* **2007**, *111*, 12906-12913.

(4) Mozzi, R. L.; Warren, B. E. The Structure of Vitreous Silica. *J. Appl. Crystallogr.* **1969**, *2*, 164-172.

(5) Brunauer, S.; Emmett, P. H.; Teller, E. Adsorption of Gases in Multimolecular Layers. *J. Am. Chem. Soc.* **1938**, *60*, 309-319.

(6) Barrett, E. P.; Joyner, L. G.; Halenda, P. P. The Determination of Pore Volume and Area Distributions in Porous Substances. I. Computations from Nitrogen Isotherms. *J. Am. Chem. Soc.* **1951**, *73*, 373-380.

(7) McClellan, A. L.; Harnsberger, H. F. Cross-Sectional Areas of Molecules Adsorbed on Solid Surfaces. *J. Colloid Interface Sci.* **1967**, *23*, 577-599.

(8) Kruk, M.; Jaroniec, M.; Sayari, A. Adsorption Study of Surface and Structural Properties of MCM-41 Materials of Different Pore Sizes. *J. Phys. Chem. B* **1997**, *101*, 583-589.

(9) Kruk, M.; Jaroniec, M.; Sakamoto, Y.; Terasaki, O.; Ryoo, R.; Ko, C. H. Determination of Pore Size and Pore Wall Structure of MCM-41 by Using Nitrogen Adsorption, Transmission Electron Microscopy, and X-ray Diffraction. *J. Phys. Chem. B* **2000**, *104*, 292-301.

(10) Yamada, S. A.; Thompson, W. H.; Fayer, M. D. Water-Anion Hydrogen Bonding Dynamics: Ultrafast IR Experiments and Simulations. *J. Chem. Phys.* **2017**, *146*, 234501.

(11) Kittaka, S.; Ishimaru, S.; Kuranishi, M.; Matsuda, T.; Yamaguchi, T. Enthalpy and Interfacial Free Energy Changes of Water Capillary Condensed in Mesoporous Silica, MCM-41 and SBA-15. *Phys. Chem. Chem. Phys.* **2006**, *8*, 3223-3231.

(12) Kou, Y.; Schmidt, S. J. Vapor Pressure and Water Activity Measurements of Saturated Salt Solutions Made with D_2O at 20°C. *Food Chem.* **1999**, *66*, 253-255.

(13) Tan, H.-S.; Piletic, I. R.; Fayer, M. D. Polarization Selective Spectroscopy Experiments: Methodology and Pitfalls. *J. Opt. Soc. Am. B* **2005**, *22*, 2009-2017.

(14) Shim, S.-H.; Zanni, M. T. How to turn your Pump-Probe Instrument into a Multidimensional Spectrometer: 2D IR and Vis Spectroscopies via Pulse Shaping. *Phys. Chem. Chem. Phys.* **2009**, *11*, 748-761.
(15) Nishida, J.; Tamimi, A.; Fei, H.; Pullen, S.; Ott, S.; Cohen, S. M.; Fayer, M. D. Structural Dynamics Inside a Functionalized Metal–Organic Framework Probed by Ultrafast 2D IR Spectroscopy. *Proc. Nat. Acad. Sci. U.S.A.* **2014**, *111*, 18442-18447.
(16) Shim, S.-H.; Strasfeld, D. B.; Fulmer, E. C.; Zanni, M. T. Femtosecond Pulse Shaping Directly in the Mid-IR using Acousto-Optic Modulation. *Opt. Lett.* **2006**, *31*, 838-840.
(17) Kumar, S. K. K.; Tamimi, A.; Fayer, M. D. Comparisons of 2D IR Measured Spectral Diffusion in Rotating Frames using Pulse Shaping and in the Stationary Frame using the Standard Method. *J. Chem. Phys.* **2012**, *137*, 184201.